# Supporting Information

# Integrative and Intermediate Self-Assembly of Multi-Walled Hybrid Nanotubes for Catanionic Biomimetics

Fenglin Liu, Wenpei Kang, ChenHao Zhao, Yunlan Su, Dujin Wang and Qiang Shen,*

## S1. Experimental Section

**Materials:** Cationic surfactant cetyltrimethylammonium hydroxide (CTAOH, 25 wt% in methanol, Shanghai Chem. Co. Ltd.), sodium dodecyl sulfate (SDS, 99.5%, Fluka), diethyl carbonate ($Et_2CO_3$, Sinopharm), methanol ($CH_3OH$, Sinopharm), calcium chloride ($CaCl_2$, Sinopharm), and ammonia solution ($NH_3 \cdot H_2O$, 25.0–28.0 wt%, Sinopharm) are of analytical grade and were used as received.

Anionic surfactant calcium dodecyl sulfate (CDS) was synthesized via the reaction between 100.0 g of SDS and 34.0 g of $CaCl_2$ in 1.0 L of deionized water. The obtained product was filtered through a cellulose acetate membrane, washed with deionized water and recrystallized three times, and dried in a vacuous desiccator at room temperature.

**Preparation of Multi-Walled Hybrid Nanotubes.** Briefly, a 25 mL of 25.3 mM CDS was slowly added to a 100 mL beaker containing the equal volume of 6.3 mM CTAOH under vigorous stirring at 60°C for 10 min, giving a total surfactant-ion concentration of $DS^-$ and $CTA^+$ at 28.4 mM and a surfactant-ion concentration ratio of $DS^-/CTA^+$ at 8.9:1.1. Then, an appropriate amount of $Et_2CO_3$ solution (1.0 M in methanol) was added into the admixture under vigorous stirring, following by the pH adjustment with the addition of $NH_3 \cdot H_2O$. Next, the reaction system was allowed to stand still at 60°C for a period of aging time, and the resulting multi-walled nanotubes of inorganic-surfactant hybrids suspended in the supernatant were directly fished out for transmission electron microscopy (TEM) observation and then for scanning electron microscopy (SEM) measurements. Finally, the precipitated inorganic-surfactant hybrid tubes were centrifugated, transferred to a vacuum drying chamber at 60°C for 2d, and then used for measurements.

It should be pointed out the finial concentration of $Et_2CO_3$ (3 ~ 9 mM), the actual pH value of reaction solutions (9.9 ~ 10.5), and the reaction time (0 ~ 15 d) were varied in order to optimize the formation of multi-walled nanotubes of inorganic-surfactant hybrids: $[Et_2CO_3]$ = 7.0 mM, pH = 10.3, reaction time = 5 d. The $DS^-/CTA^+$ surfactant-ion concentration ratio was fixed at 8.9:1.1 and the total

surfactant-ion concentration of $DS^-$ and $CTA^+$ was set at a constant of 28.4 mM. Also, in order to demonstrate the mineralization-driven (i.e., purpose- or function-driven) self-assembling processes of calcium-loaded catanionic surfactants for the formation of the multi-walled nanotubular architectures, the same reaction systems in the absence of $Et_2CO_3$ were conducted and treated as experimental controls.

**Characterization:** SEM measurements were performed on a JEOL JSM-6700F scanning electron microscope, fitted with a field emission source and operating at an accelerating voltage of 15 kV. The precipitated sample was firstly dispersed in ethanol via ultrasonic treatment for 10 min and then deposited on a copper stage, while the suspended sample was directly deposited on a copper stage, dried and treated with platinum-sputtering prior to SEM measurements.

For TEM studies, the dispersed samples were prepared by mounting a drop of a solution on a carbon coated Cu grid and allowed to dry in air, while the precipitated sample was firstly dispersed in ethanol via ultrasonic treatment for 10 min and then transferred onto a carbon coated Cu grid. These unstained samples were observed using the JEM-100CX11 transmission electron microscope operating at 100 kV and the high-resolution TEM (HR TEM) operating at 200 kV.

The X-ray diffraction (XRD) patterns of lyophilized suspensions and/or centrifugated precipitates were performed on a Rigaku D/max-2400 powder X-ray diffractometer with Cu Kα radiation (40 kV, 120 mA). The 0.08° steps/(25 s) and the 2θ range from 0 to 60° were selected to analyze the phase structures of inorganic-organic hybrids or crystals.

## S2. Roles of the Surfactant Hydrophobic Interactions

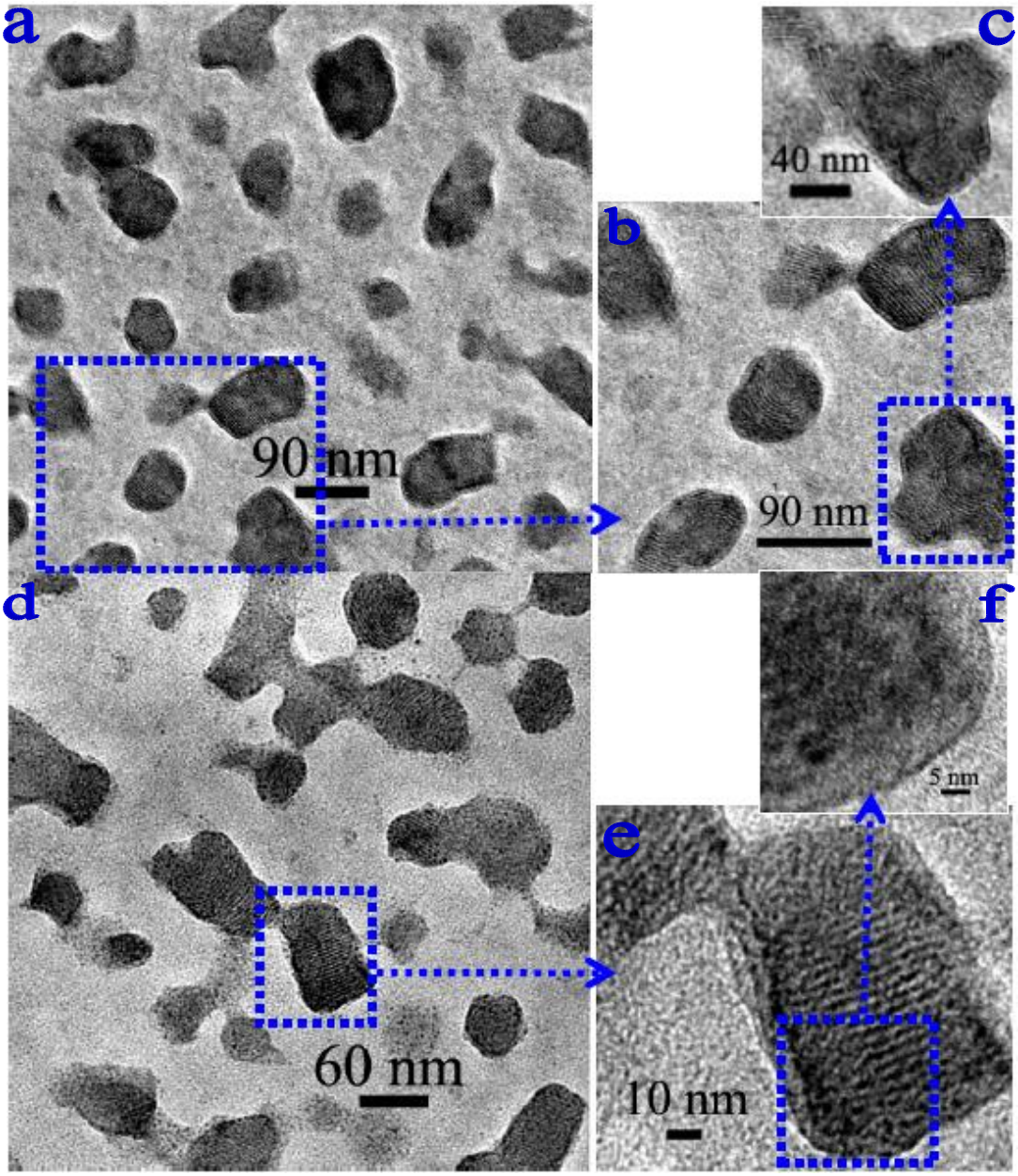


**Fig.S1.** TEM images of the $Ca(OH)_2$-catanionic surfactant hybrids constructed by mixing the equal volume of 6.3 mM CTAOH and 25.3 mM CDS solutions (final pH, 10.3) rapidly, displaying the gradual disappearance of inorganic-organic nanolamellae under the irradiation of electron beams. The dash rectangular regions marked in panels (a) and (d) were magnified and shown in panels (b) and (e), respectively, showing clearly an onion-like structure. The dash rectangular regions marked in panels (b) and (e) were magnified and shown in panels (c) and (f), respectively, indicating the amorphous nature of nanolayered hybrids.

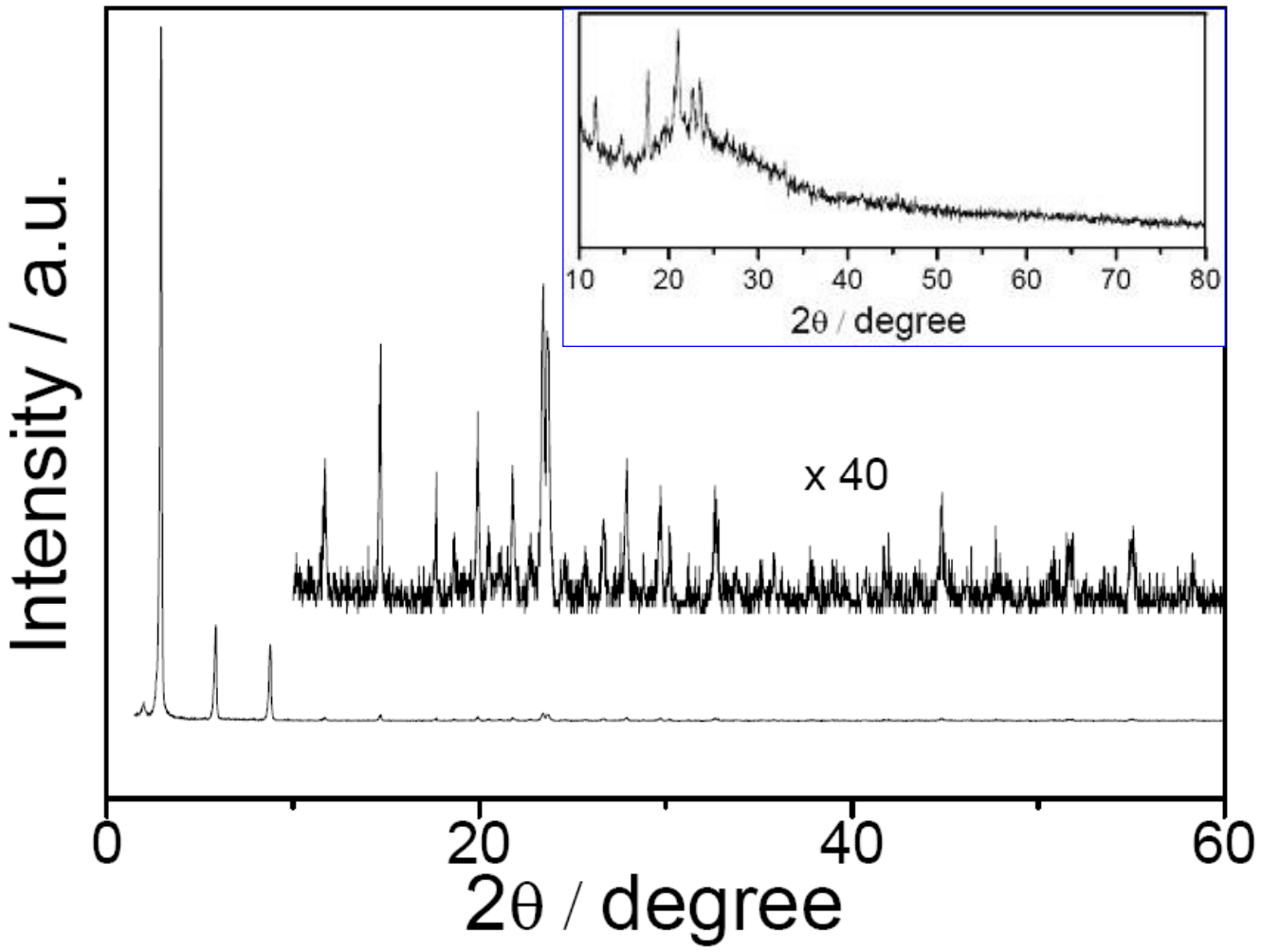


**Fig.S2.** XRD profile of the lamellar $Ca(OH)_2$-catanionic surfactant hybrids constructed by mixing the equal volume of 6.3 mM CTAOH and 25.3 mM CDS solutions (final pH, 10.3) rapidly. The top-right inset is the XRD profile of the powder mixture of cetyltrimethylammonium bromide and sodium dodecyl sulfate. The middle inset is the selected part of forty-time magnified XRD pattern (from 10 to 60°), showing also the [00*l*] ($l \geq 4$) reflections of the lamellar $Ca(OH)_2$-catanionic surfactant hybrids with a separation of ~3.02 nm. In contrast to the extended length of surfactant hydrocarbon chains (i.e., ~1.8 nm for CDS and ~2.5 nm for CTAOH), the interbedded catanionic surfactants were attributed to be the cross-stacked bilayer through the hydrophobic interactions of hydrocarbon chains. In the middle inset, other XRD reflection peaks could be assigned to the uncertain reflections of surfactants, not the crystalline calcium hydroxide, which could be visually determined by the XRD profiles of the powdered surfactant mixtures (top-right inset).

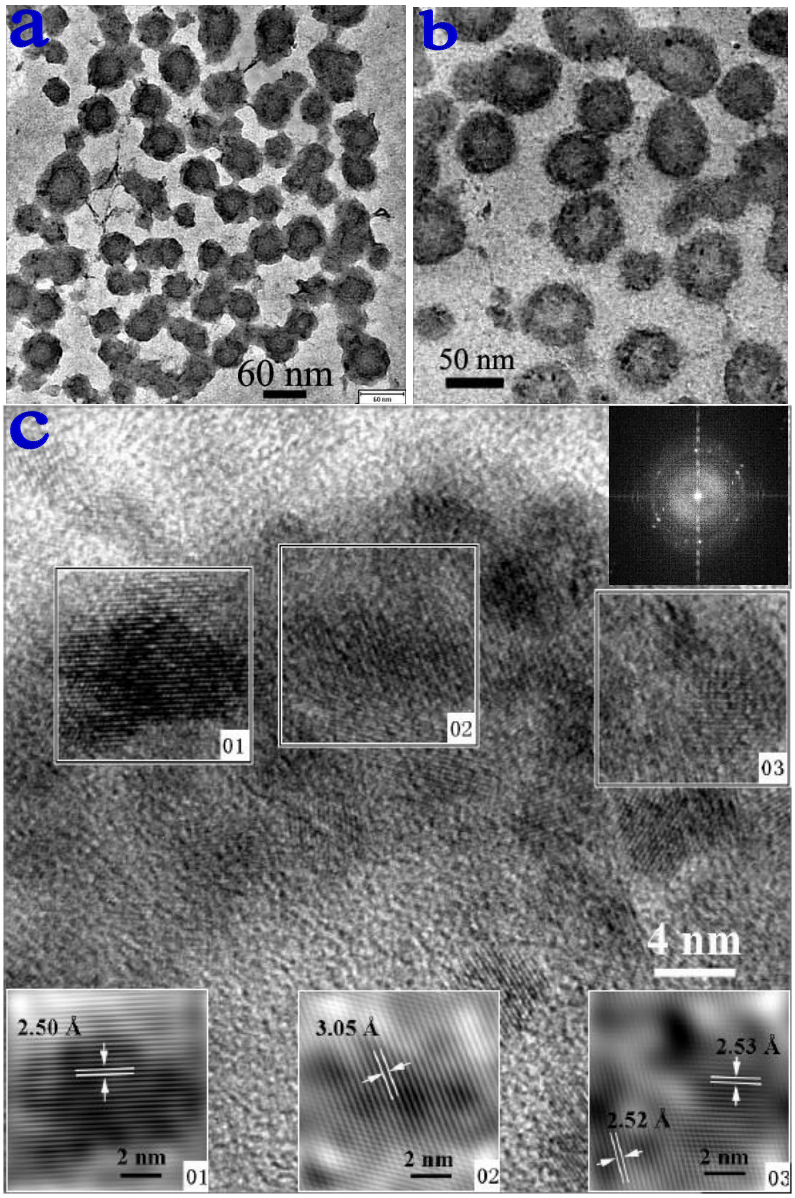


**Fig.S3.** (a, b) Low- and (c) high-resolution TEM images of unstained hollow nanospheres of calcium-loaded catanionic surfactants generated in the dilute system (pH = 10.3) of 0.1 mM CTAOH + 1.0 mM CDS + 0.4 mM $Et_2CO_3$ at a reaction time of 15 d. The inset at the upper right corner of panel (c) is the corresponding Fourier transform pattern, indicating the polycrystalline nature of nanospheres and the lamellar feature of spherical shells. In panel (c), the numbered regions were magnified, filtered, and shown also as insets downstairs, assigned to the calcite crystal faces of (110) or (104) with an interplaner spacing of 2.50 Å or 3.04 Å (JCPDS 05-0586), respectively. In terms of the traditional phase separation model of surfactant micelles formed in a dilute solution, the polymeric nature of previously formed $Ca(OH)_2$, its encapsulation action outside surfactant micelles, and the template effectiveness of nanospherical shells for the formation of calcite nanocrystals, were emphasized simultaneously.

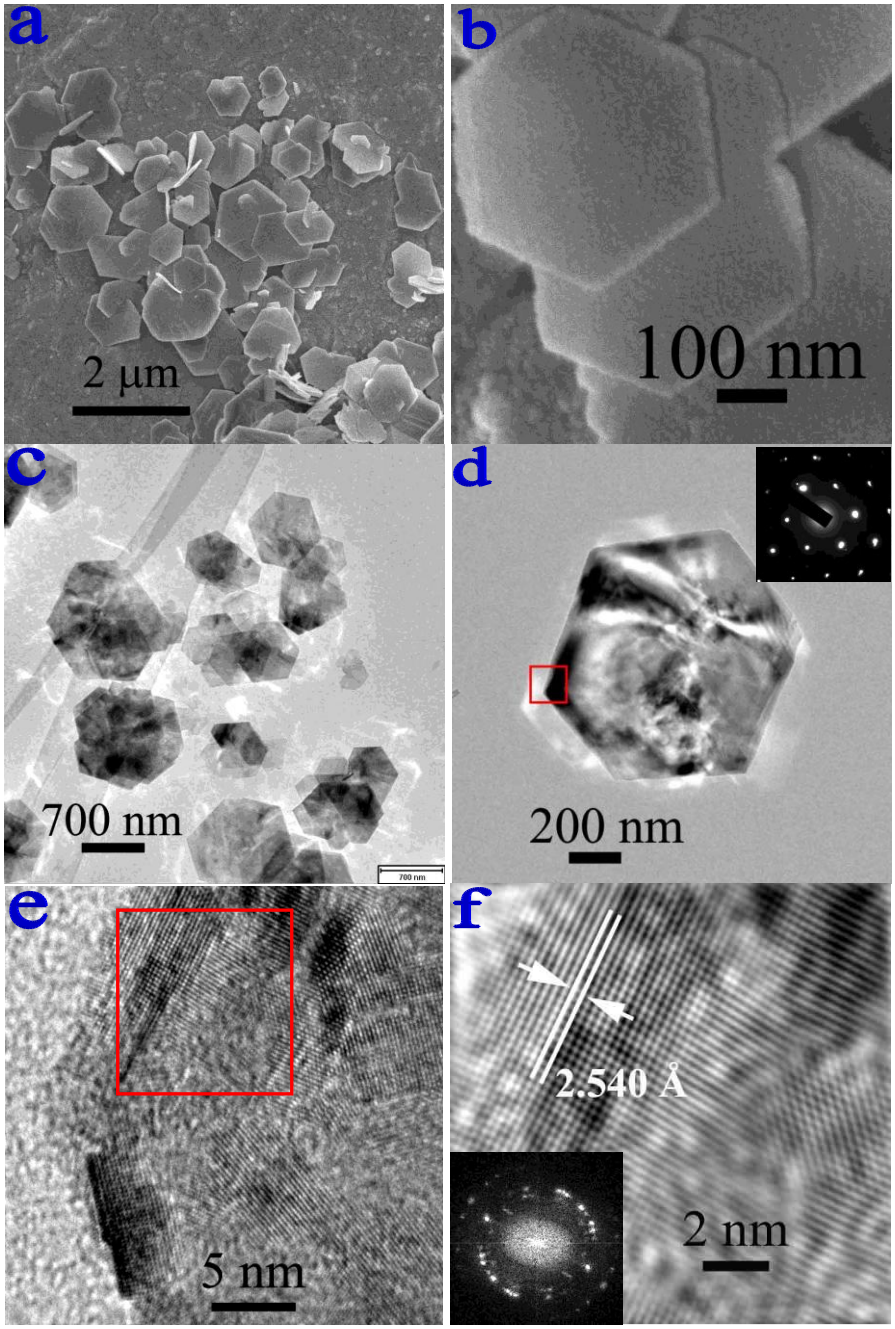


**Fig.S4.** (a, b) SEM, (c, d) TEM, and (e, f) HRTEM images of mesocrystals precipitated from the concentrated reaction systems (pH = 10.3) of 3.2 mM CTAOH + 12.7 mM CDS + 7.0 mM $Et_2CO_3$ at the reaction time of 15 days, suggesting the surfactant-assisted self-assembly of inorganic nanocrystals for the formation of a mesocrystal. In panel (d), the selected square was magnified and shown in panel (e), indicating that the calcite platelet is composed of tiny nanocrystals. Panel (f) is the magnified and filtered picture of the selected region marked by a red square in panel (e), and the calcite crystal plane of (110) with an interplaner spacing of 2.540 Å was labeled therein. Insets in panels (d) and (f) are the corresponding SAED pattern and Fourier transform, indicating the "single-" and poly-crystalline nature respectively.

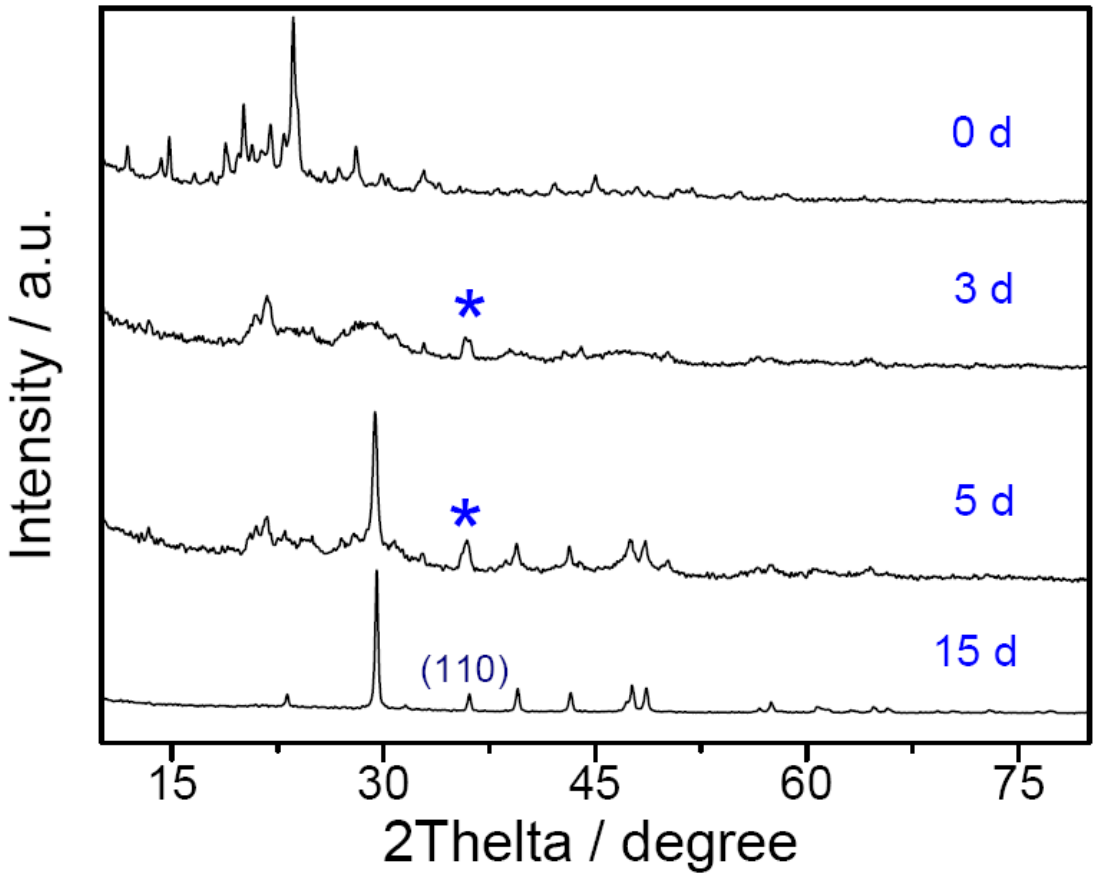


**Fig.S5.** XRD profiles of samples obtained from the concentrated reaction systems (pH = 10.3) of 3.2 mM CTAOH + 12.7 mM CDS + 7.0 mM $Et_2CO_3$ at different reaction times of 0, 3, 5, and 15 d. The XRD pattern of lyophilized reaction suspension, sampled immediately after mixing, shows almost the same characteristics as that of powdered surfactant admixture of cetyltrimethylammonium bromide and sodium dodecyl sulfate shown in Fig.S2. From that time on, precipitation occurred in the reaction systems through the gradually base-catalyzed hydrolysis of $Et_2CO_3$. By comparison, it could be concluded that, with the increase of reaction time, the interbedded catanionic surfactants gradually desorbed from the precipitates owing to the increasing consumption of calcium ions. At the reaction time of 3 or 5 d, the XRD patterns of precipitates show clearly the asterisk-marked reflection peaks of calcite crystal faces of (110) at the 2-theta angles of 36.0°. Also, the full width at half maximum (FWHM) of an individual peak suggests the tiny nanometer-scaled nature of calcite in comparison with these of the final product sampled at the reaction interval of 15 d.

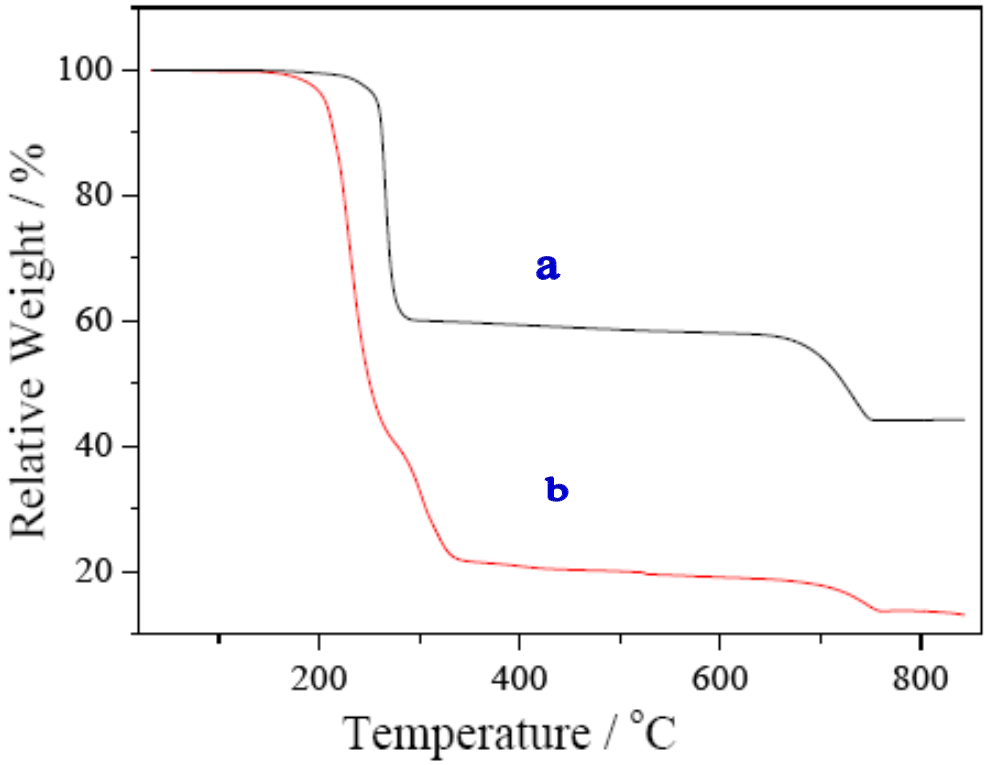


**Fig.S6.** Thermogravimetric analysis (TGA) curves of (a, black) the precipitates, sampled from the reaction system (pH = 10.3) of 3.2 mM CTAOH + 12.7 mM CDS + 7.0 mM $Et_2CO_3$ at the reaction time of 5 d, and (b, red) the corresponding reaction system without the addition of $NH_3 \cdot H_2O$ (pH adjustment) and in the absence of $Et_2CO_3$, lyophilized immediately after the mixing of 25.3 mM CDS (25 mL) and 6.3 mM CTAOH (25 mL). It should be mentioned that TGA measurements were performed on a METTLER thermogravimetric analyzer at a heating rate of 10 °C/min from room temperature to 850°C under a nitrogen atmosphere. For the precipitated intermediates of multi-walled nanotubes (a), the ~39.5 wt% mass loss below 280°C (defined as the first decomposing process) could be assigned to the degradation of surfactant hydrocarbon chains, while the second decomposing process exhibits ~16.1 wt% weight loss prior to 747°C, which can be attributed to the decomposition of inorganic calcium salts (e.g., the previously formed $CaCO_3$ and unreacted $Ca(OH)_2$) to produce CaO. By comparison, for the lyophilized admixture of CDS and CTAOH solutions (b), the relatively high weight loss during the first decomposing process could be explained using the incomplete precipitation of catanionic surfactants. Also, the relatively low weight loss during the second thermal decomposition (B) was due to the incomplete consumption of CDS without the addition of $NH_3 \cdot H_2O$ and $Et_2CO_3$.

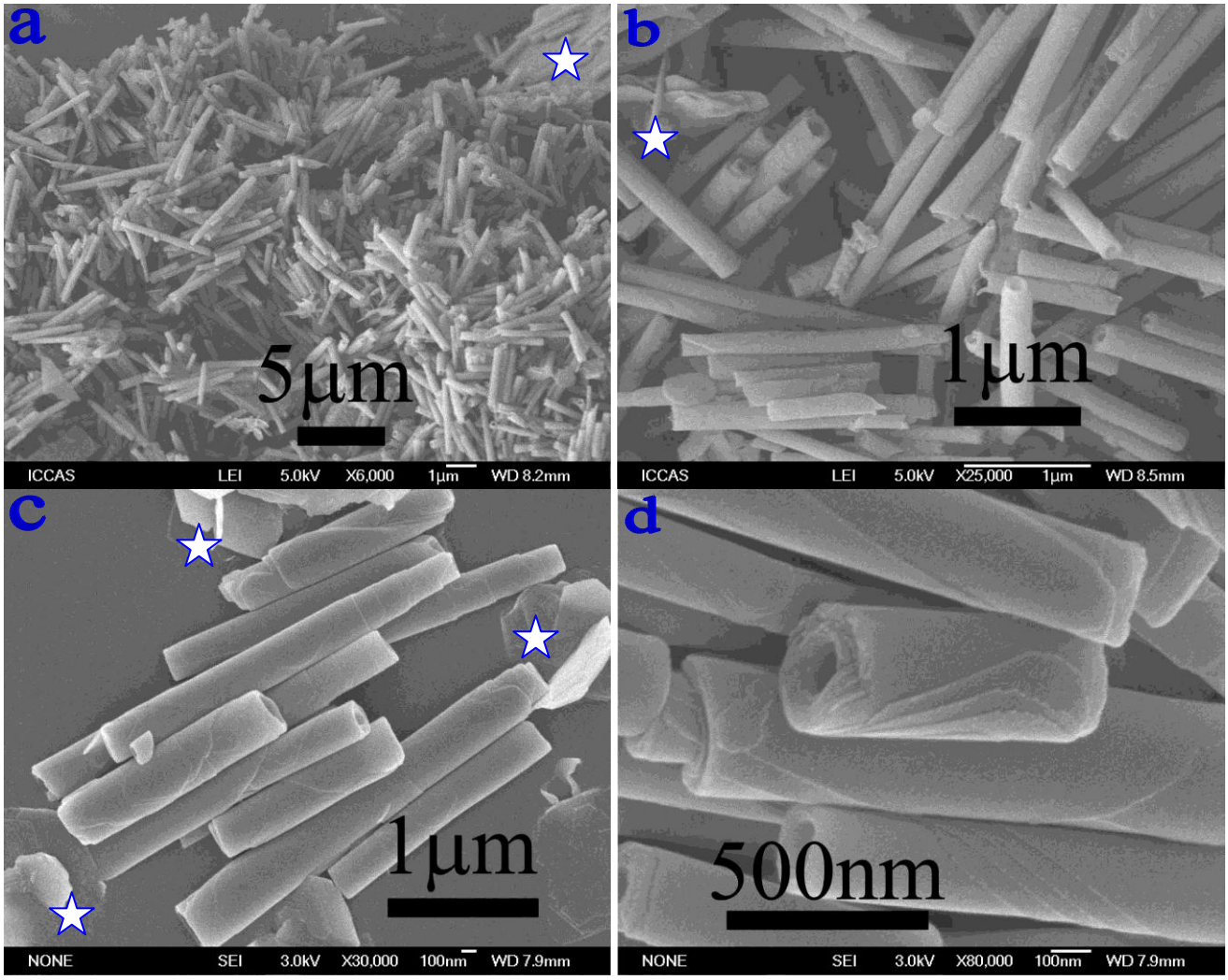


**Fig.S7.** SEM images of the self-organized architectures of calcium-loaded catanionic surfactants precipitated from the reaction systems (pH = 10.3) of 3.2 mM CTAOH + 12.7 mM CDS + 7.0 mM $Et_2CO_3$ at the reaction time of 5 d, showing gradually the paper-rolled tubular shapes with an open-ended structure. In panels (a), (b) and (c), the nanometer-sized platelets marked by pentagon symbols could be assigned to the in-situ generated calcite particles, according to the final and unique products shown in Fig.S4. This also indicates that the reaction interval of ~ 5 d is both the maturity-time limit for the dynamic growth of multi-walled hybrid nanotubes and the beginning-limit for the dynamic disappearance of these intermediates.

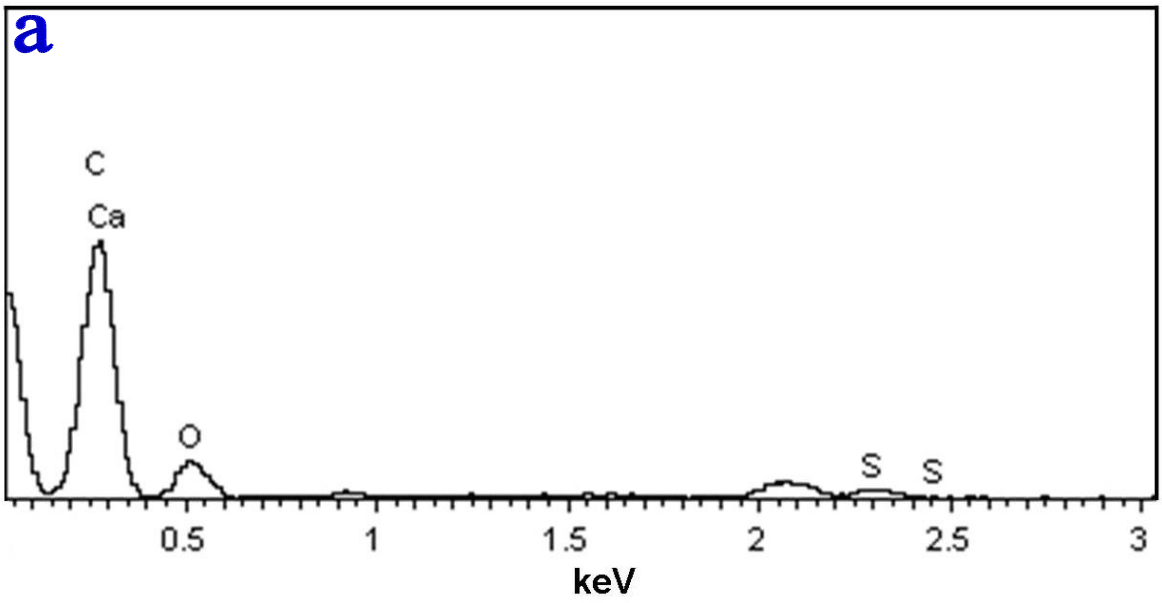


b

| Sample 1 | | | Sample 2 | | | Sample 3 | | |
|---|---|---|---|---|---|---|---|---|
| Element/K | Weight% | Atomic% | Element/K | Weight% | Atomic% | Element/K | Weight% | Atomic% |
| C | 66.69 | 73.65 | C | 64.04 | 71.24 | C | 61.94 | 69.41 |
| O | 30.65 | 25.41 | O | 33.33 | 27.83 | O | 35.10 | 29.53 |
| S | 0.68 | 0.28 | S | 0.63 | 0.26 | S | 0.76 | 0.32 |
| Ca | 1.97 | 0.65 | Ca | 2.01 | 0.67 | Ca | 2.20 | 0.74 |

**Fig.S8. (a)** A representative energy dispersive spectrum (EDS) of multi-walled hybrid nanotubes self-organized by the calcium-loaded catanionic surfactant hybrids in the supernatant of reaction systems (pH = 10.3) of 3.2 mM CTAOH + 12.7 mM CDS + 7.0 mM $Et_2CO_3$ at the reaction time of 5 d. **(b)** EDS results obtained by focusing electron beam on different multi-walled hybrid nanotubes shown in panel (c) of Fig.S7. These show that the major C and O elements and the minor Ca and S elements are detected, suggesting that the grown nanotubes are mainly composed of organic surfactants.

## S3. Dynamic Growth and Disappearance of Multi-Walled Hybrid Nanotubes

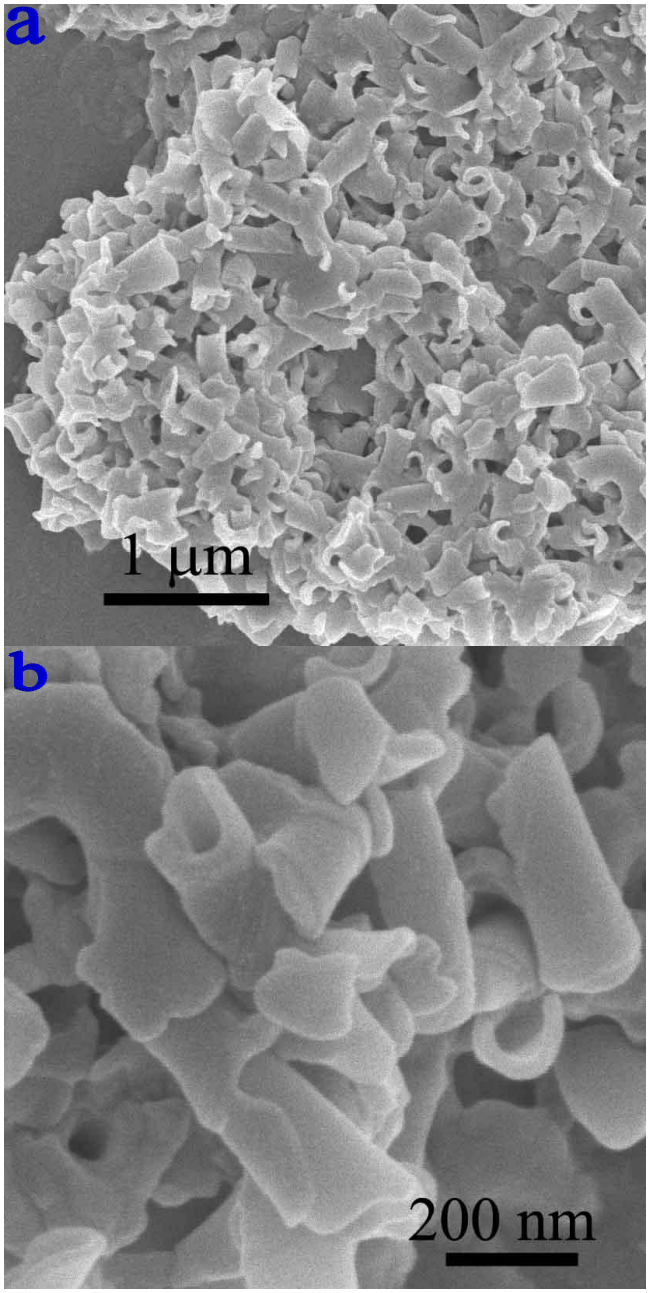


**Fig.S9.** SEM images of the air-dried calcium-loaded catanionic surfactant hybrids fished out of the freshly prepared suspension (pH = 10.3) of 3.2 mM CTAOH + 12.7 mM CDS + 7.0 mM $Et_2CO_3$, and the reaction time was defined as 0 day (ibid). Panel (a) shows the irregular sheet-like structure of the calcium-loaded catanionic surfactant hybrids, while panel (b) is the magnified SEM picture of panel (a), showing the self-curling characteristics of sheet-like hybrids.

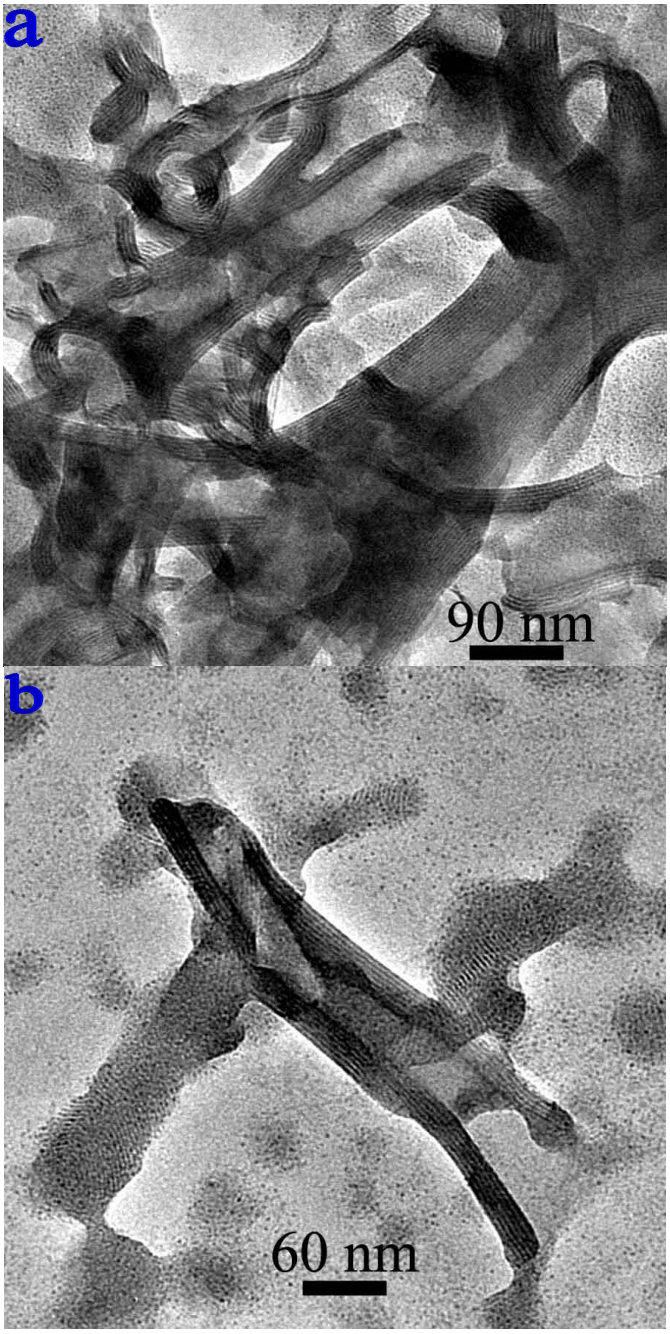


**Fig.S10.** HR TEM images of the air-dried calcium-loaded catanionic surfactant hybrids fished out of the freshly prepared suspension (pH = 10.3) of 3.2 mM CTAOH + 12.7 mM CDS + 7.0 mM $Et_2CO_3$, showing the partly straightening feature of lamellar catanionic surfactant-$Ca(OH)_2$ precursors in the presence of $Et_2CO_3$. In contrast to the catanionic surfactant-$Ca(OH)_2$ precursors shown in Fig.S1, the water-insoluble $Et_2CO_3$ solubilized in surfactant hydrophobic regions caused the interplanar spacing to increase from 3.02 to 3.34 nm. Panel (b) displays also the coexistence of a multi-walled nanotube embryoa and the irregular aggregates of nanolamellated calcium-loaded catanionic surfactant hybrids.

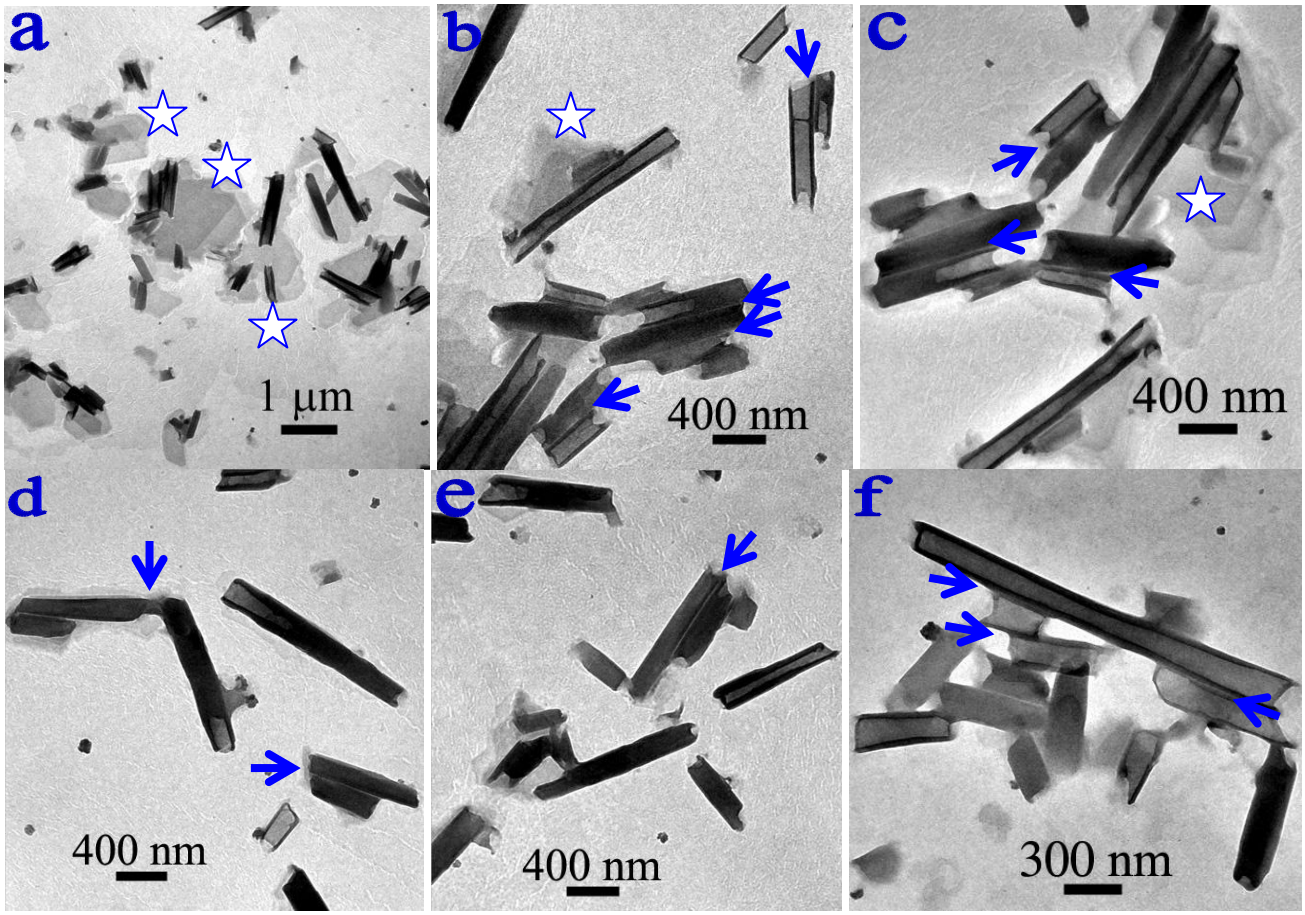


**Fig.S11.** TEM images of lyophilized tubular architectures of calcium-loaded catanionic surfactant hybrids self-organized in the reaction systems (pH = 10.3) of 3.2 mM CTAOH + 12.7 mM CDS + 7.0 mM $Et_2CO_3$ at the reaction interval of 3 d. The pentagon symbols exhibit the nanolamellated structures of unrolled calcium-loaded catanionic surfactant hybrids with irregular shapes, while the arrows indicate the orienting ordered arrangement of tubular architectures through the polymerization/hydration nature of unreacted $Ca(OH)_2$ and the hydrophobic interactions of surfactant hydrocarbon chains.

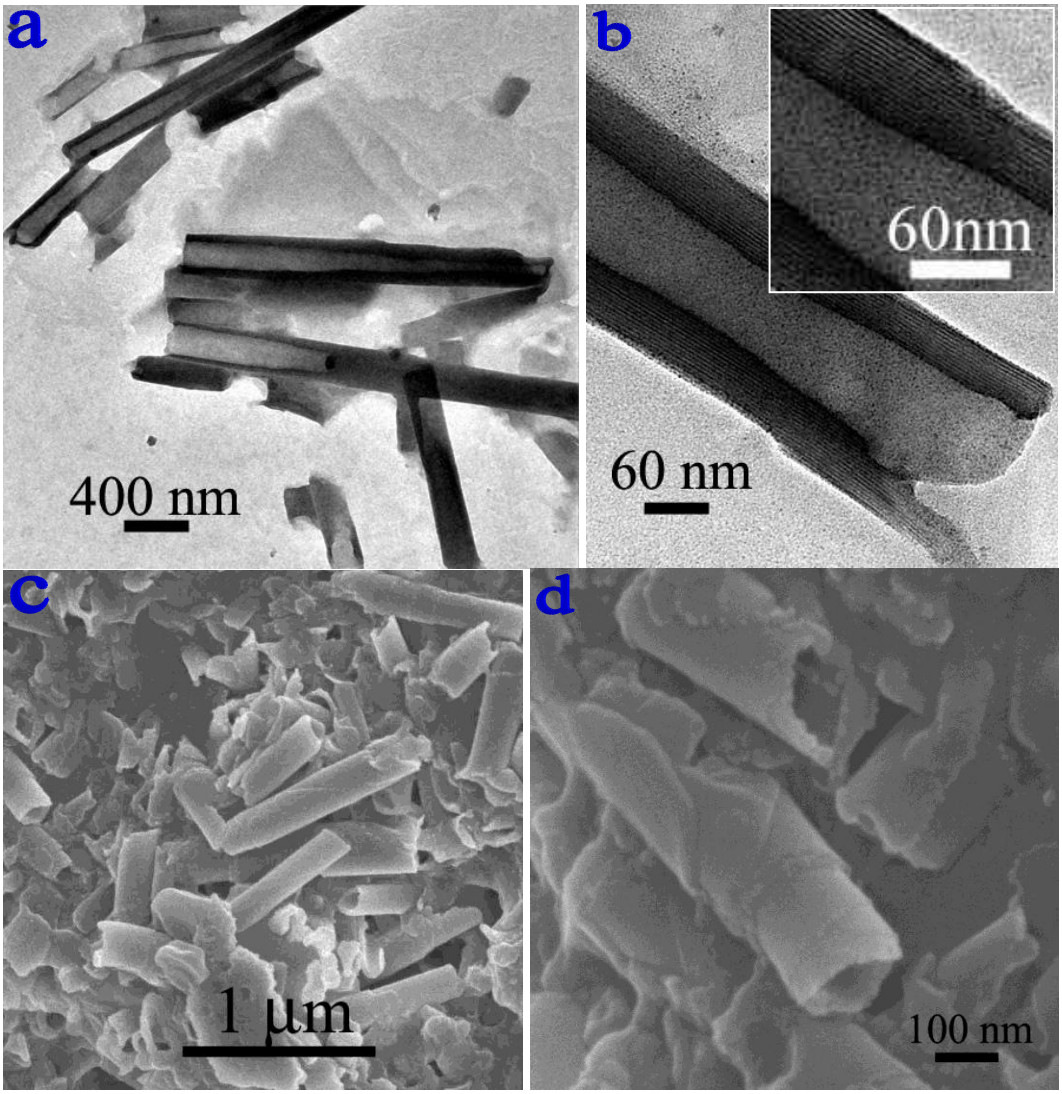


**Fig.S12.** (a, b) TEM and (c, d) SEM images of lyophilized multi-walled nanotubes of the calcium-loaded catanionic surfactant hybrids self-organized in the supernatant of reaction systems (pH = 10.3) of 3.2 mM CTAOH + 12.7 mM CDS + 7.0 mM $Et_2CO_3$ at the reaction time of 5 d. Inset in panel (b) is a relatively high magnification view of the corresponding tube wall, giving the lamellar structure with a fringe interspacing of ~3.34 nm. The magnified SEM picture (i.e., panel d) shows the paper-rolling arrangement of calcium-loaded catanionic surfactant sheets for the formation of multi-walled hybrid nanotubes, suggesting also the exfoliation manner of tubular architectures in the sedimentary phases after the complete consumption of $Et_2CO_3$.

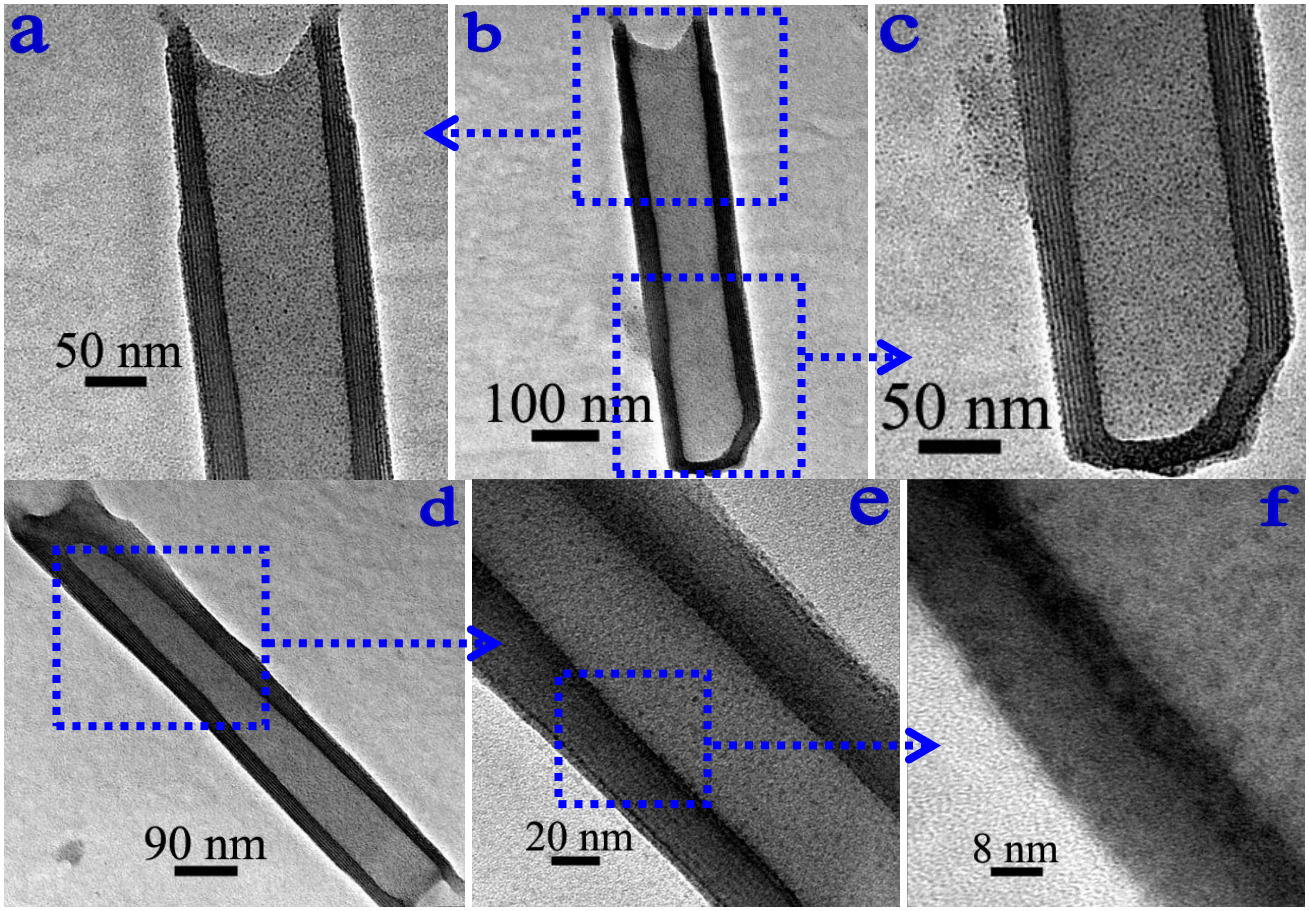


**Fig.S13.** TEM images of occasionally observed tubular architectures of the calcium-loaded catanionic surfactant hybrids self-organized in the supernatant of reaction systems (pH = 10.3) of 3.2 mM CTAOH + 12.7 mM CDS + 7.0 mM $Et_2CO_3$ at the reaction time of 5 d, showing the multi-walled structures with one open end and another closed end. Panels (a) and (c) are the magnified pictures of the nanotube shown in panel (b), displaying the irregular thickness and nanolamellated structure of the tubular wall. In panel (c), the polygonal shape of closed tubular end indicates also the incorporation of polymeric inorganics (i.e., $Ca(OH)_2$ and $CaCO_3$) into catanionic surfactant layers. Panels (e) and (f) are the gradually magnified pictures of the nanotube shown in panel (d), showing the gradually vague characteristics of tubular wall under the increasing irradiation of electron beams. Also, this indicates that the sizes of calcite nanocrystals formed in-between catanionic surfactant sheets are too small to be detected.

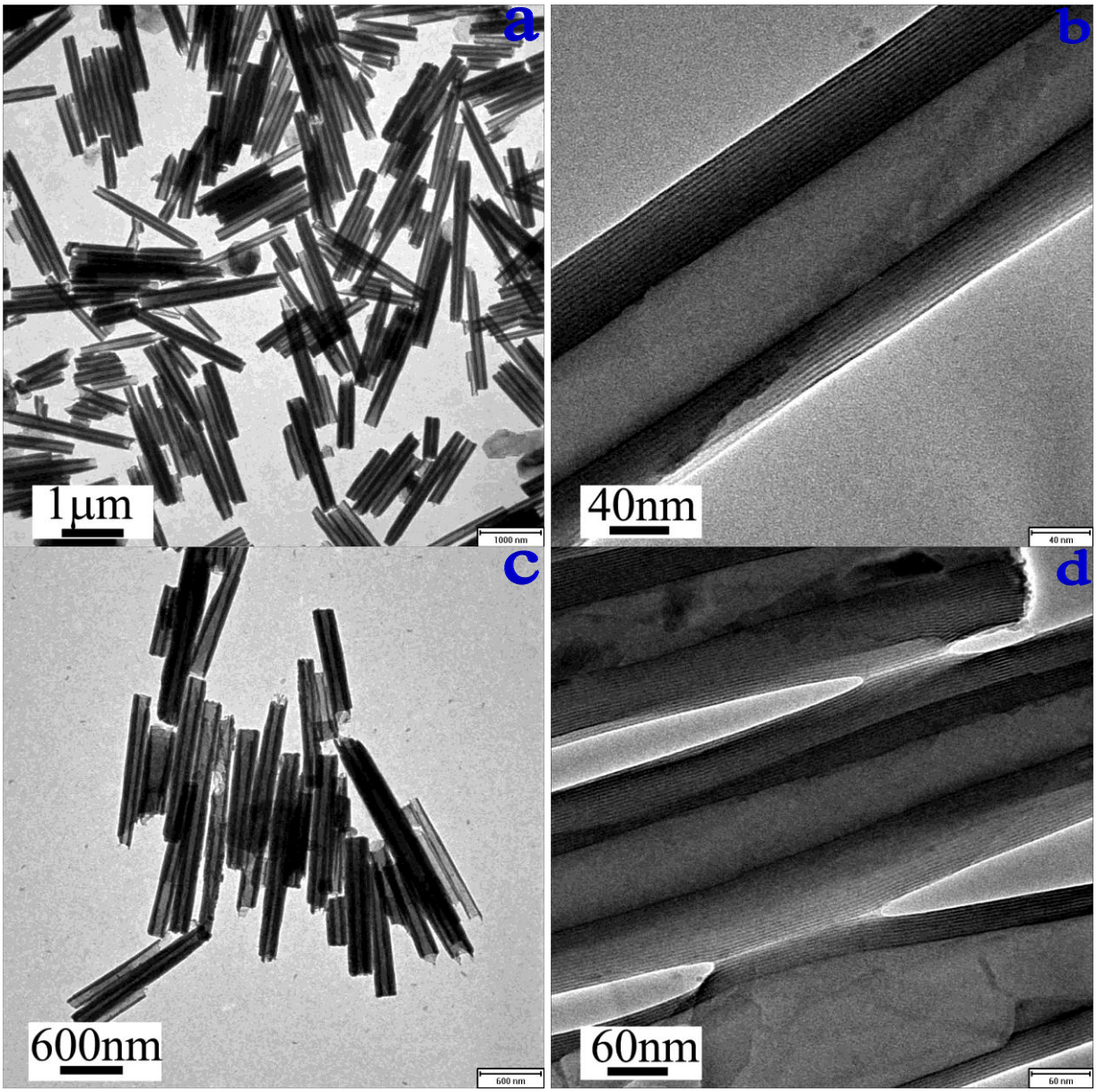


**Fig.S14.** TEM images of self-organized architectures of the calcium-loaded catanionic surfactants precipitated from the reaction systems (pH = 10.3) of 3.2 mM CTAOH + 12.7 mM CDS + 7.0 mM $Et_2CO_3$ at the reaction time of 5 d, showing the multi-walled tubular shapes with an open-ended structure. In panel (a), one of the nanotubes was magnified and shown in panel (b), suggesting that the driven forces for the formation of multi-walled nanotubes are the polymeric nature of inorganic calcium salts (i.e., $Ca(OH)_2$ and $CaCO_3$) and the hydrophobic interactions of surfactant hydrocarbon chains. In panel (c), parts of the two-dimensional nanotube array were magnified and shown in panel (d), indicative of the orienting ordered arrangement of nanotubes.

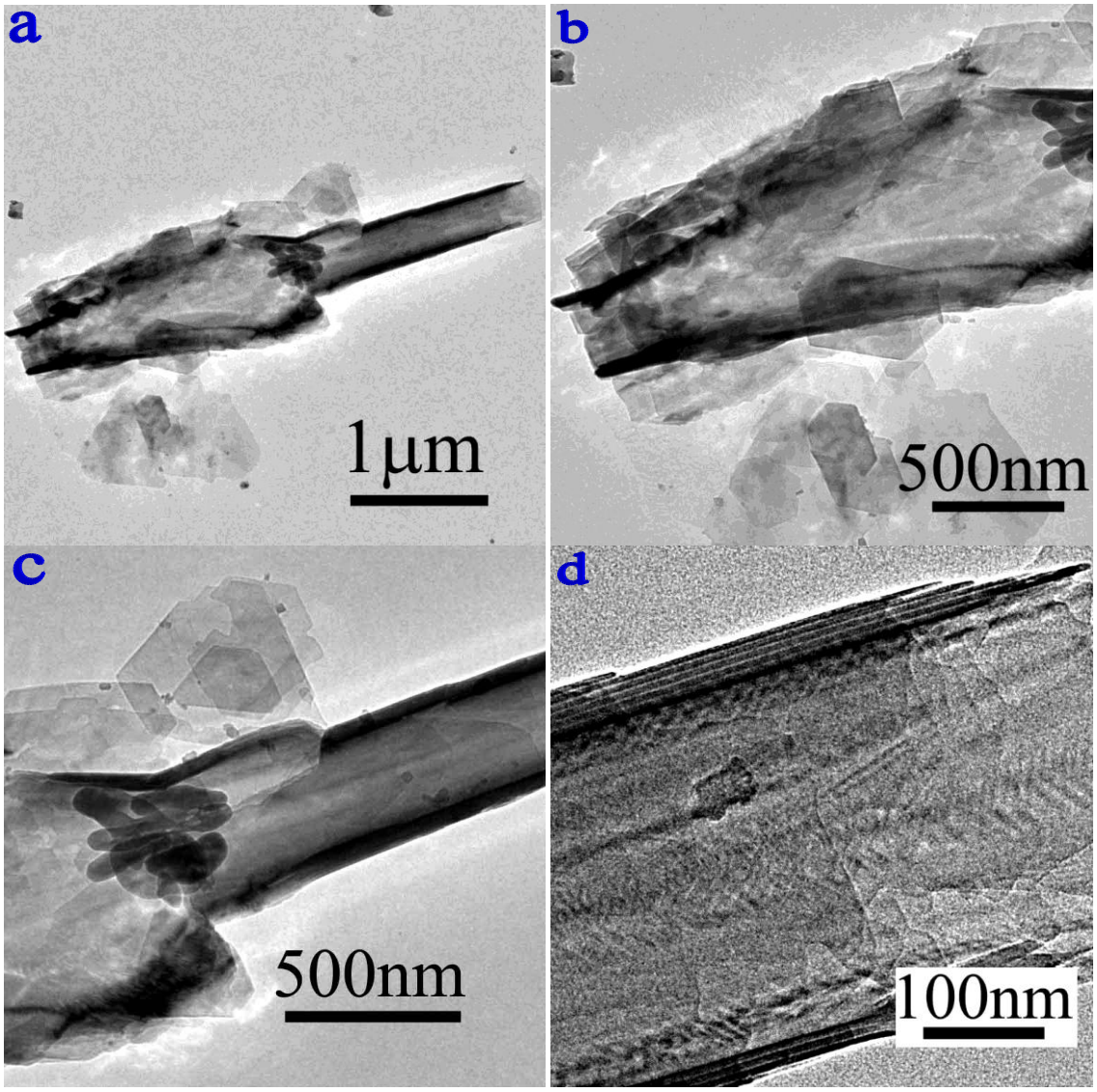


**Fig.S15.** (a) TEM image of a partly broken multi-walled nanotube of calcium-loaded catanionic surfactant hybrids captured occasionally in the sedimentary phases of 3.2 mM CTAOH + 12.7 mM CDS + 7.0 mM $Et_2CO_3$ at the reaction time of 10 d. (b–d) The magnified TEM images of the broken multi-walled nanotube. Panels (b) and (c) indicate the kinetically breaking phenomena of tubular walls and their coexistence of the simultaneously generated hexagonal platelets of calcite. Panel (d) shows the morphology of the relatively "unchanged" tubular end, and the corresponding Fourier transformation estimates the interlayer spacing at a value of ~ 6.68 nm, twice as big as that of a growing nanotube (~3.34 nm) shown in Fig.S7 or S13. By comparison, the double interlayer spacing indicates the completely swelling of cross-stacked surfactant bilayer, suggesting also the breaking manner (or, the vanishing pathway) of these multi-walled hybrid nanotubes.

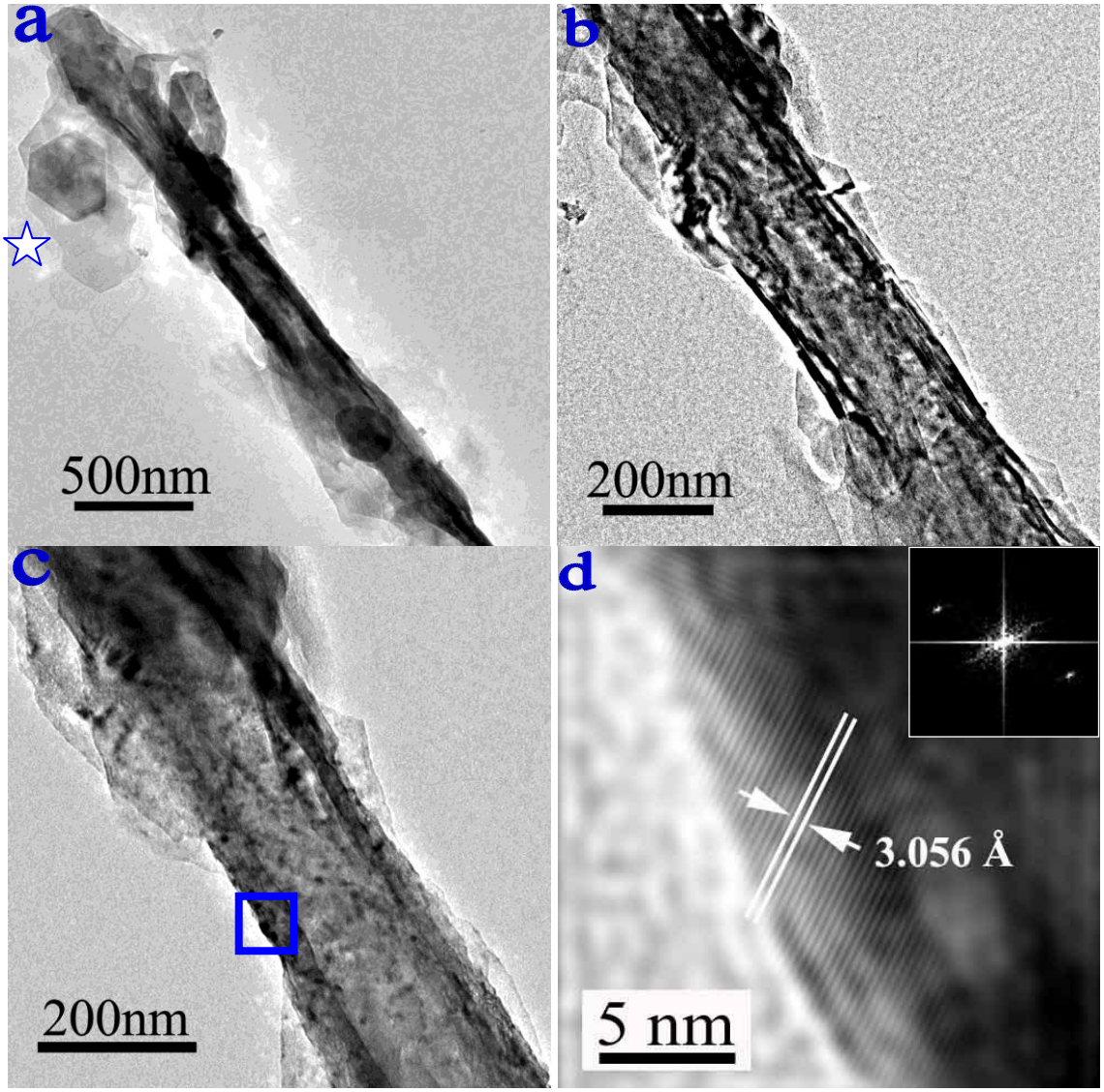


**Fig.S16.** (a) TEM image of a shrinking multi-walled nanotube of calcium-loaded catanionic surfactant hybrids captured occasionally in the sedimentary phase of 3.2 mM CTAOH + 12.7 mM CDS + 7.0 mM $Et_2CO_3$ at the reaction time of 10 d, showing its coexistence with the simultaneously generated hexagonal calcite platelets. (b, c) TEM images of the gradually magnified multi-walled nanotube, displaying the distorted and broken morphology and the irradiated dehydration of tubular walls, respectively. (d) High-resolution TEM image of the square region marked in panel (c), and the inset is the corresponding Fourier transform pattern, showing the (104) crystal face of calcite with an interplanar spacing of 0.306 nm.

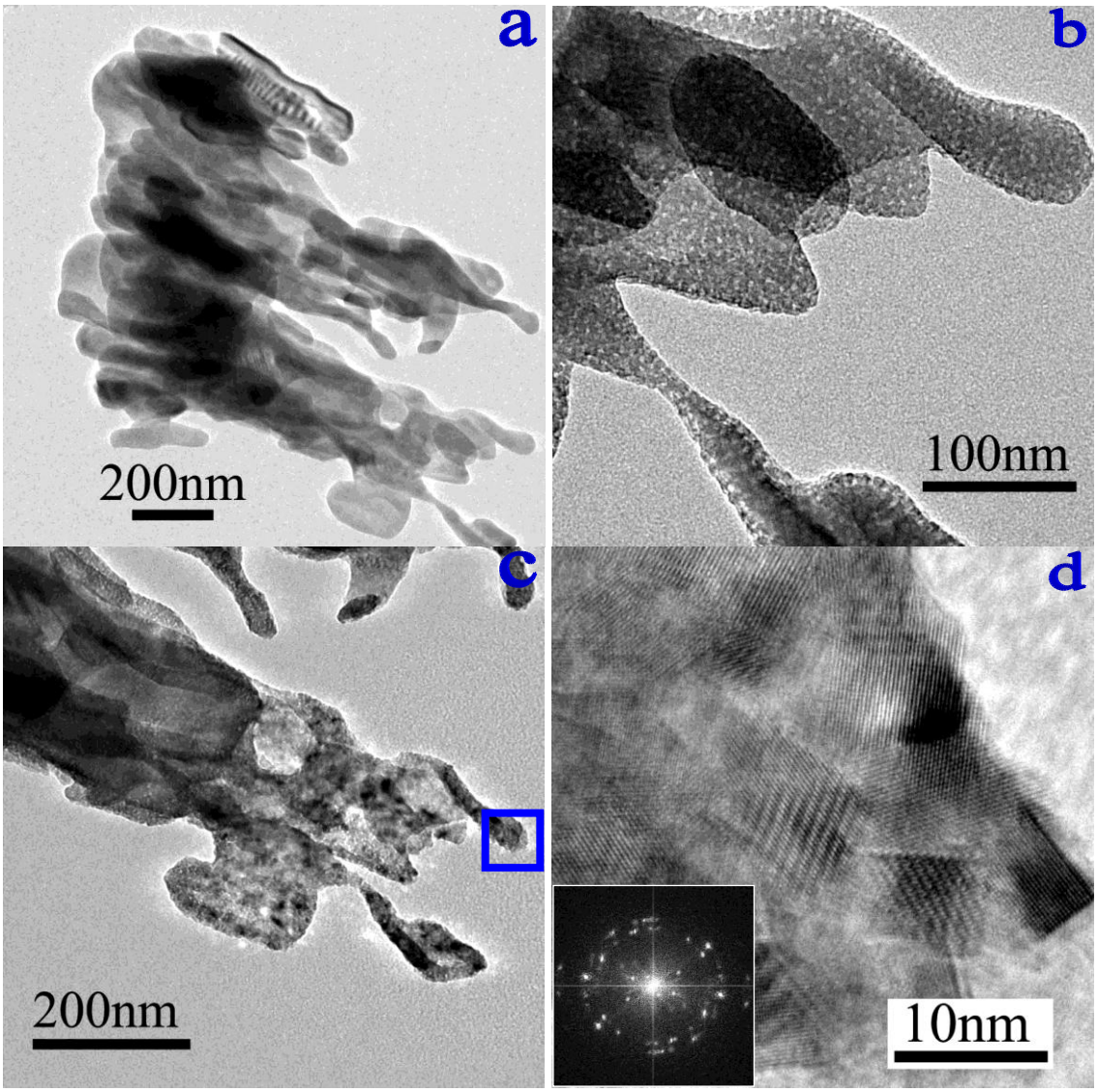


**Fig.S17.** (a–d) The gradually magnified TEM images of a possibly vanishing two-dimensional array of multi-walled hybrid nanotubes captured occasionally in the sedimentary phases of 3.2 mM CTAOH + 12.7 mM CDS + 7.0 mM $Et_2CO_3$ at the reaction time of 10 d. Under the irradiation of electron beam, the dehydration of curling hybrid sheets were clearly observed, shown in panels (b) and (c). Panel (d) is the high-resolution TEM image of the square region marked in panel (c), and inset is the corresponding Fourier transform pattern, indicating the polycrystalline nature of vanishing tubular walls. In comparison with the Fourier transform pattern of a growing nanotube shown above, panel (d) and the inset suggest also that the crystallization of calcium carbonate occurs during the disappearance stage of multi-walled hybrid nanotubes.

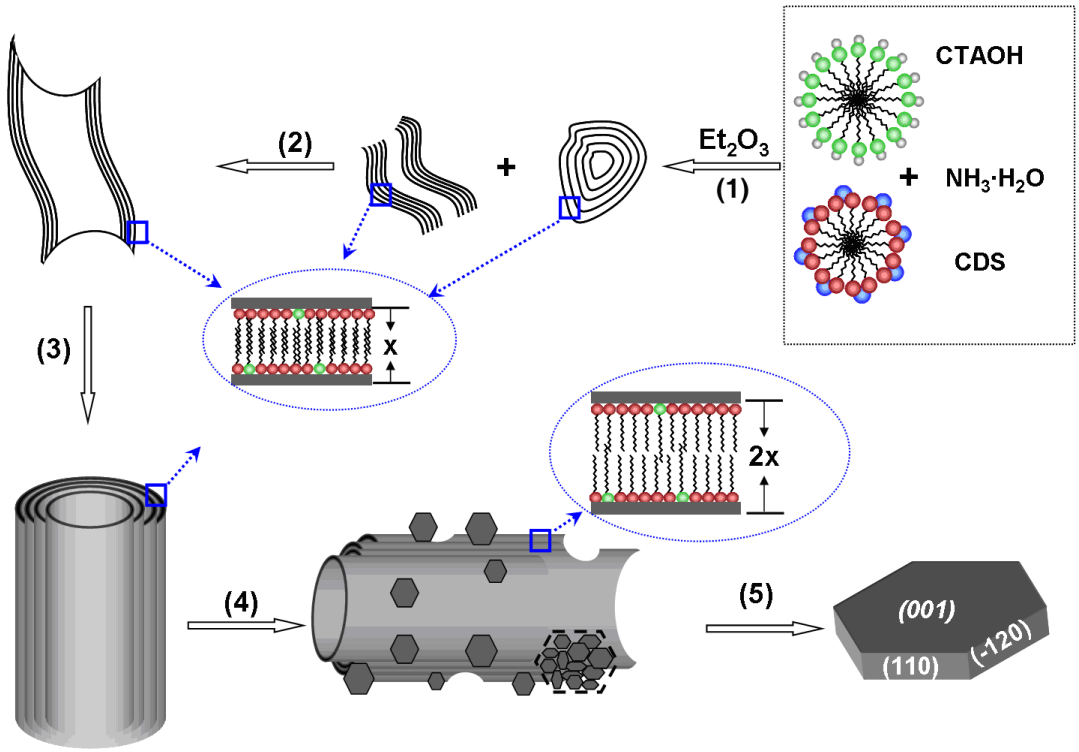


**Fig.S18.** A schematic drawing summarizes the dynamic growth and disappearance of multi-walled calcium-loaded catanionic surfactant hybrid nanotubes during the biomimetic fabrication of hexagonal calcite platelets: **(1),** the addition of diethyl carbonate $Et_2CO_3$ into previously mixed catanionic systems induced the fusing of onion-like structures, resulting in infant multi-walled nanotubes and multilayered vesicles; **(2),** the self-curling of nanolayered $Ca(OH)_2$-catanionic surfactant precursors (spacing ~3.02 nm) resulted in multi-walled tubular architectures with twisted walls and ends; **(3),** a small sum of in situ formed calcite nanocrystals break the long-range order of bilayered hydrocarbon chains, extend and straighten calcium-loaded catanionic surfactant tubes, resulting in grown tubular intermediates with a wall spacing of ~ 3.34 nm; **(4),** the continuously base-catalyzed hydrolysis of $Et_2CO_3$ (i.e., the chemical transformation of $Ca(OH)_2$ to $CaCO_3$ by resulting $CO_2$ gas and the swelling of resulting ethanol) at inorganic-organic interfaces alters the geometric packing parameters of tubular intermediates, resulting in calcite platelets and broken tubes with a wall separation of ~6.68 nm; **(5),** the self-assembled nanocrystals induced the formation of hexagonal calcite platelets with a "single-crystalline" nature.